

Structure-Based Design of Novel Pyrimido[4,5-c]pyridazine Derivatives as Dihydropteroate Synthase Inhibitors with Increased Affinity

Ying Zhao,^[a] Dalia Hammoudeh,^[b] Mi-Kyung Yun,^[b] Jianjun Qi,^[c] Stephen W. White,^[b, d] and Richard E. Lee^{*[a, c]}

Dihydropteroate synthase (DHPS) is the validated drug target for sulfonamide antimicrobial therapy. However, due to widespread drug resistance and poor tolerance, the use of sulfonamide antibiotics is now limited. The pterin binding pocket in DHPS is highly conserved and is distinct from the sulfonamide binding site. It therefore represents an attractive alternative target for the design of novel antibacterial agents. We previously carried out the structural characterization of a known pyridazine inhibitor in the *Bacillus anthracis* DHPS pterin site and identified a number of unfavorable interactions that appear to compromise binding. With this structural information, a series of 4,5-dioxo-1,4,5,6-tetrahydropyrimido[4,5-c]pyridazines were designed to improve binding affinity. Most im-

portantly, the *N*-methyl ring substitution was removed to improve binding within the pterin pocket, and the length of the side chain carboxylic acid was optimized to fully engage the pyrophosphate binding site. These inhibitors were synthesized and evaluated by an enzyme activity assay, X-ray crystallography, isothermal calorimetry, and surface plasmon resonance to obtain a comprehensive understanding of the binding interactions from structural, kinetic, and thermodynamic perspectives. This study clearly demonstrates that compounds lacking the *N*-methyl substitution exhibit increased inhibition of DHPS, but the beneficial effects of optimizing the side chain length are less apparent.

Introduction

Since their discovery in the 1930s, the sulfonamide class of drugs (sulfa drugs) has been widely used for the treatment of a broad spectrum of infectious diseases.^[1,2] These drugs target the essential folate pathway in microorganisms, and combinations with dihydrofolate reductase (DHFR) inhibitors such as trimethoprim have proven highly effective in treating *E. coli* urinary infections, *Pneumocystis carinii* infections in immune-compromised patients and community-acquired methicillin-resistant *Staphylococcus aureus* (MRSA).^[3,4] Sulfa drugs target dihydropteroate synthase (DHPS), an enzyme encoded by the *folP* gene that acts at a key convergent point in folate biosynthesis,^[5] and mutations in the *folP* gene are associated with sulfa drug resistance. Resistance mutations have now been reported and characterized in many organisms, including drug-resistant forms of *S. aureus* and *P. carinii*; this phenomenon, together with frequent severe side effects associated with allergenicity,^[6,7] have become critical issues for the continued use of sulfa drugs as antimicrobials. Therefore, to continue to take advantage of this valuable drug target, there is an urgent need for the development of alternatives to sulfa drugs that avoid resistance and overcome their poor tolerability.

To date, crystal structures of DHPS from many microbial sources have been resolved, including complexes with substrate and product analogues.^[8–15] The sulfa drugs mimic the substrate *para*-aminobenzoic acid (*p*ABA) and bind at the *p*ABA binding site, composed of two flexible loop regions which can readily accommodate mutations that confer sulfa drug resistance.^[11,16] In contrast, the second substrate dihy-

dropterin pyrophosphate (DHPP; Figure 1) binds in the 7,8-dihydropterin binding pocket, deep within the highly conserved DHPS β barrel, in which sulfa drug resistance mutations have never been observed. The pterin binding site is therefore a very attractive alternative target for the design and development of novel antimicrobial agents, and our research group has been pursuing this goal.^[17,18]

One of the more potent pterin-pocket-targeted inhibitors that we have encountered is a pyridazine compound that was originally discovered by researchers at Burroughs Wellcome in

[a] Dr. Y. Zhao,⁺ Prof. R. E. Lee
Department of Chemical Biology and Therapeutics
St. Jude Children's Research Hospital
262 Danny Thomas Place, Mail Stop 1000
Memphis, TN 38105 (USA)
E-mail: Richard.lee@stjude.org

[b] Dr. D. Hammoudeh,⁺ M.-K. Yun, Prof. S. W. White
Department of Structural Biology
St. Jude Children's Research Hospital
262 Danny Thomas Place, Mail Stop 311
Memphis, TN 38105 (USA)

[c] Dr. J. Qi, Prof. R. E. Lee
Department of Pharmaceutical Sciences
University of Tennessee Health Science Center, Memphis, TN 38163 (USA)

[d] Prof. S. W. White
Department of Microbiology, Immunology and Biochemistry
University of Tennessee Health Science Center, Memphis, TN 38163 (USA)

[*] These authors contributed equally to this work.

Supporting information for this article is available on the WWW under <http://dx.doi.org/10.1002/cmdc.201200049>.

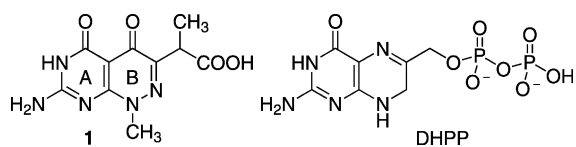


Figure 1. Structure of pyridazine inhibitor **1** and substrate DHPP.

the late 1970s.^[19,20] However, improvement was not possible due to the lack of structural information on the complex between this compound and DHPS. We subsequently determined the crystal structure of *Bacillus anthracis* DHPS (*Ba*DHPS) in complex with this molecule **1** (Figure 1) and confirmed that it does engage the pterin pocket.^[21] The pyridazine pterin-like scaffold binds within the actual pocket as predicted, and the carboxyl side chain partially occupies the anion pocket that normally accommodates the pyrophosphate moiety of the substrate.

The crystal structure revealed that the A ring of **1** engages the pterin pocket in a similar fashion to the actual pterin substrate DHPP, through key interactions with conserved residues Asp184 and Asn120 (Figure 2a).^[9,21] Although the second B ring is more structurally divergent from the pterin substrate, the 5-carbonyl group of **1** mimics the hydrogen-bond-accepting N5 nitrogen of DHPP to form a strong hydrogen bond with the conserved Lys220. Elsewhere, the interactions are less ideal with two notable examples: the exocyclic carboxyl group attached to the pyridazine 6-position forms an apparently strained salt bridge with Arg254, and the methyl group at the 8-position prevents the N8 nitrogen atom from making a favorable hydrogen bonding interaction with the conserved Asp101, as observed in the pterin pyrophosphate (PtPP) and DHPP complex structures.^[9,16] Using a ligand-docking-based approach to design and explore further analogues, we demonstrated that removal of the N8-methyl group and optimization of the C6 carboxylate side chain should facilitate an optimal binding mode that more accurately mimics the binding of DHPP.^[13,21] In the current study we designed and synthesized new 2-aminopyrimido[4,5-*c*]pyridazines and tested whether they do indeed maximize these interactions, resulting in improved DHPS inhibitors.

Results

Chemistry

In the first compound series the exocyclic C6 carboxylic acid side chain was systematically varied; this group was chemically accessible via simple modifications of existing synthetic schemes. The first molecule targeted was compound **5**, in which the carboxylate was placed directly adjacent to the ring system. Direct cyclization of 2-amino-6-chloropyrimidin-4(3*H*)-one **6** with diethyl 2-oxomalonate did not give the desired 4,5-dioxopyridazine, but instead produced the 3,5-dioxo analogue.^[20] Therefore, compound **5** was obtained by an alternate route in which 2,4-diamino-6-chloropyrimidine **2** was treated with methylhydrazine in boiling water to give compound **3**,

which was condensed with diethyl 2-oxomalonate to give bicyclic compound **4**. Simultaneous C4 deamination and saponification of **4** in hot aqueous sodium hydroxide followed by acidification afforded the target compound **5** (Scheme 1).

In the next set of side chain variants, the carboxylate group was progressively extended away from the ring system by the addition of methyl branched or unbranched methylene spacers. These compounds **16–18** were obtained from 2-amino-6-chloropyrimidin-4(3*H*)-one **6** with the treatment of methylhydrazine in boiling water followed by condensation with the appropriate diethyl α -keto ester to give compounds **9–11**, respectively. Saponification of **9–11** in aqueous sodium hydroxide followed by acidification afforded **16–18** (Scheme 2).^[20]

The synthesis of the N8-demethyl analogues proved to be more demanding. Initial attempts to directly demethylate the N8 position of **16** and **18** using β -(trimethylsilyl)ethyl chloroformate were unsuccessful.^[22] We therefore adopted a benzyl protecting group strategy for N8. Benzylated 7-amino-1-benzylpyrimido[4,5-*c*]pyridazine-4,5(1*H*,6*H*)-diones **12–15** were synthesized from **6** with benzylhydrazine by using a similar approach as described for **9–11**.

Direct debenzoylation and de-esterification of **13** was carried out by reaction with aluminum trichloride in boiling toluene (Scheme 3) to afford **19** in moderate yield. However, attempts to extend this methodology to synthesize the other targeted analogues failed due to poor reaction yields and difficulty in separating the product from aluminum salt by-products.

This led us to apply selective hydrogenolysis as an alternative strategy to perform debenzoylation (Scheme 4).^[23] Intermediates **12**, **14**, and **15** were subject to debenzoylation using formic acid and 10% palladium on carbon to give demethylated esters **20–22**,^[23] and these esters were subsequently saponified with aqueous sodium hydroxide to afford the target compounds **23–25**, respectively.

Enzyme inhibition studies

Compounds **5**, **16–19**, and **22–25** were all tested for the inhibition of *Ba*DHPS by using a previously developed endpoint radiometric product detection assay (Table 1).^[21] Compounds **16–18** and **5** directly probe the side chain moiety relative to the parent compound **1**. Removal of the branched methyl side chain from **1** resulted in compound **16** with a ~50% poorer IC_{50} value, mirroring the effect of methyl branch substitution in the N8-demethylated pair **19/23**. Compounds **17/18** and **24/25** have an extra methylene side chain spacer relative to the respective parent compounds **1** and **19**, and this was observed to give rise to decreased inhibitory activity. For both the **17/18** and **24/25** pairs, the inhibitors that are methyl branched (**18** and **25**) were weaker than the unbranched compounds **17** and **24**; this stands in contrast to the effects observed for the shorter chain branching pair of **1** and **16**. The inhibitory activity of compound **5**, in which the carboxylic acid is directly connected to the bicyclic ring, dropped dramatically relative to the initial compound **1** and showed no detectable IC_{50} value.

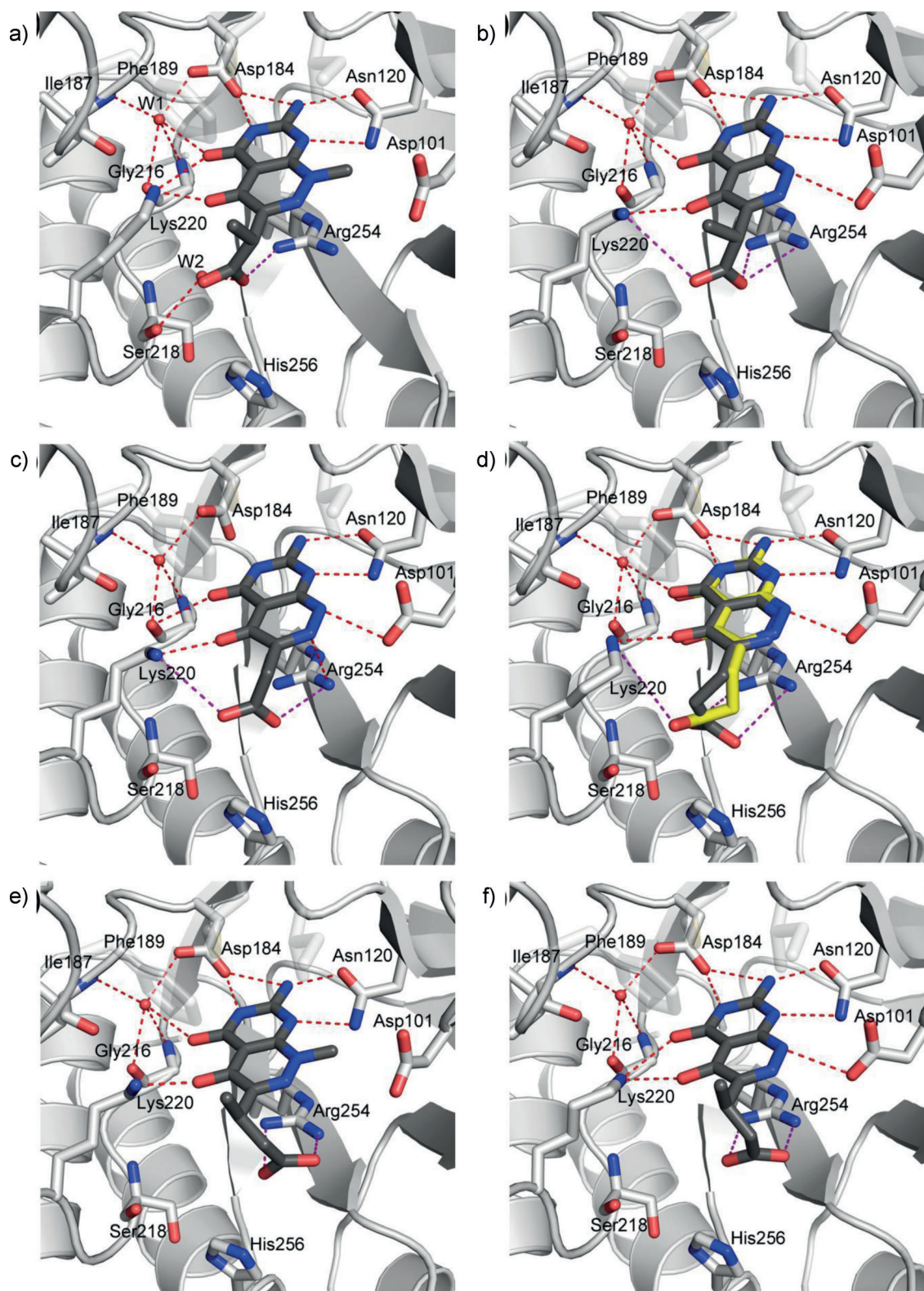
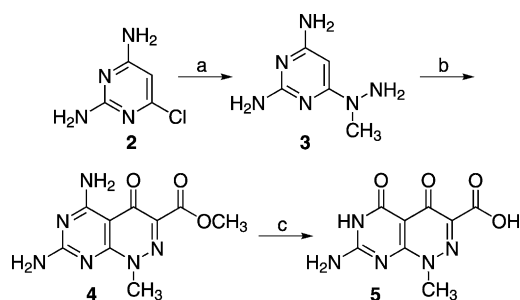


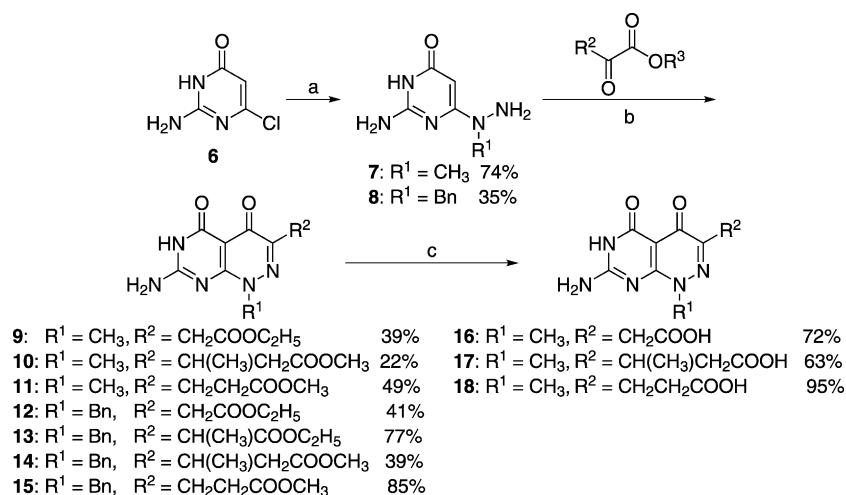
Figure 2. Crystal structures of complexes between *Ba*DHPS and pyridazine-derived inhibitors. a) Details of the interactions of compound **1** with key residues within the pterin binding site of *Ba*DHPS.^[21] Similar representations for compounds b) **19**, c) **23**, d) **25***, e) **17**, and f) **24**. *Compound **25** binds in two conformations within the *Ba*DHPS dimer, and these are superimposed in the figure.

Therefore, from this section of the study, the side chain substitution of **1** appears optimal.

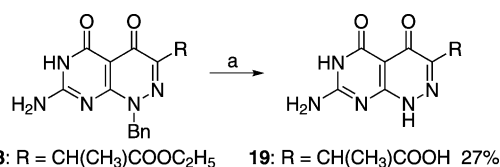
Compounds **19** and **23–25** probe the removal of the N8-methyl group relative to **1** and **16–18**, respectively. All of the demethylated compounds showed improved inhibition over



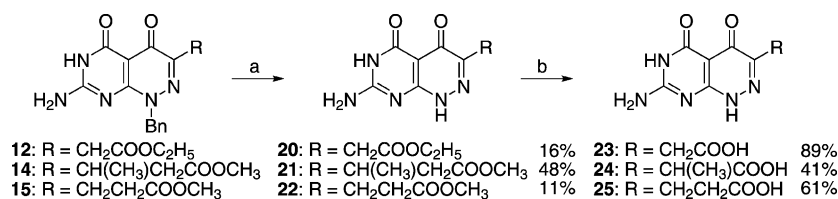
Scheme 1. Reagents and conditions: a) CH_3NHNH_2 , H_2O , reflux, 5 h, 27%; b) diethyl 2-oxomalonate, CH_3OH (anhyd), reflux, 3 days, 44%; c) 1. 1 N NaOH, RT, overnight, 2. HCl, 47%.



Scheme 2. Reagents and conditions: a) CH_3NHNH_2 , H_2O , reflux, 5 h, or $\text{BnNHNH}_2 \cdot 2\text{HCl}$, Et_3N , H_2O , reflux, overnight; b) H_2O or CH_3OH , reflux; c) 1. 1 N NaOH, RT, overnight, 2. HCl.



Scheme 3. Reagents and conditions: a) AlCl_3 , PhCH_3 , 100°C , 3 h.



Scheme 4. Reagents and conditions: a) HCOOH , 10% Pd/C; b) 1. 1 N NaOH, RT, overnight, 2. HCl.

their corresponding methylated analogues, and compounds **19** and **23** showed greater inhibition than the parent compound **1**. Finally, to expand the SAR of the pyridazine analogues, a number of synthetic intermediates were also tested for inhibitory activity. The saponification products of N8-benzylated analogues **12–15** lacked significant enzyme inhibition (data not shown), consistent with the binding pocket at the N8 position being unable to accommodate a bulky substituent such as

a benzyl group. The preference for a free terminal carboxylic acid was also confirmed by comparing the inhibitory activity of ester **22** with its free acid **25**.

Thermodynamic and kinetic analyses

The binding affinities of the most potent derivatives compared with that of **1** were further examined with respect to thermodynamics and binding kinetics using isothermal titration calorimetry (ITC) and surface plasmon resonance (SPR). Both techniques showed that all six compounds bind to *Ba*DHPS at a 1:1 molar ratio with respect to the DHPS monomer (Table 2; see Supporting Information figures S1–S3 for the specific ITC binding isotherms and SPR kinetic

binding profiles). Comparing the N-methylated and demethylated pairs **1/19**, both the ITC and SPR data show an approximate two-fold increase in affinity upon demethylation. ITC reveals that the increase in free energy of binding of **19** over **1** results from an increased entropic contribution, which overcompensates for some loss to the enthalpy of binding.^[24] With regard to the **16/23** pair, it was not possible to determine binding by ITC, but SPR shows a similar twofold level of improved binding upon removal of the N8-methyl group. ITC and SPR both show that increasing the side chain length in compounds **24** and **25** substantially decreases binding affinity, and SPR reveals that there is a pronounced and undesirable increase in the disassociation rate. A comparison between methyl-substituted **24** and straight-chain **25** analogues shows that the methyl substitution is disfavored overall; it is more entropically favored, but significantly penalized in enthalpic terms. Overall, the data from these experiments agree well with the results obtained from the enzyme assays (Table 1).

Structural analyses

In the published crystal structure of the **1**–DHPS complex, a network of hydrogen bonding interactions between Asn 120, Asp 184, a structured water molecule (W1) and Lys220 anchors the A ring to the pterin binding pocket in a similar fashion to PtPP and DHPP (Figure 2a; see Supporting Information figure S5 for the complex between the DHPP analogue PtPP and *Ba*DHPS).^[9,16] The B ring is bound via hydrogen bonding interactions with Lys220 and a second structured water molecule (W2), a salt bridge between the acetate group of the small molecule and Arg254, van der Waals interactions

Table 1. *Ba*DHPS inhibitory activities of pyridazines.

| Compd | Structure | Inh. [%] ^[a] | IC ₅₀ [μM] ^[b] | Compd | Structure | Inh. [%] ^[a] | IC ₅₀ [μM] |
|-------|-----------|-------------------------|--------------------------------------|-------|-----------|-------------------------|-----------------------|
| 1 | | 97.0 | 22 | 19 | | 95.3 | 11 |
| 16 | | 96.0 | 32 | 23 | | 91.0 | 18 |
| 17 | | 52.5 | 145 | 24 | | 75.8 | 57 |
| 18 | | 65.0 | ND | 25 | | 91.8 | 36 |
| 5 | | 32.4 | ND | 22 | | 33.0 | 260 |

[a] Enzyme inhibitory activity determined at a test compound concentration of 250 μM. [b] ND: not determined.

between the methyl group of the linker and Phe189, and the methyl group at position 8 with the β carbon atom of Asp101 (Figure 2 a).

We first structurally characterized the complex with **19** to directly observe the effect of removing the N8-methyl group (Figure 2 b). The A ring is bound in the pterin pocket by an identical constellation of hydrogen bonding interactions, except that the hydrogen bond between the 4-oxo group and Lys220 is missing. As predicted from the substrate analogue complex,^[21] the effect of removing the N8-methyl group from the B ring is to allow the resulting NH group to form a hydrogen bond with the side chain of Asp101, which rotates to optimize this interaction. Regarding the carboxylate side chain, its interactions with Arg254 within the anion binding pocket and with Phe189 via the branching methyl group are largely unchanged. A small but significant effect of removing the N8-methyl group is that the pterin-like ring structure rotates and moves to accommodate the new interaction with Asp101. Superimposing the complexes of compounds **1** and **19** with respect to the protein backbone shows this subtle movement and the rotation of Asp101 (Figure 3 a).

Compared with **19**, compound **23** only lacks the methyl group in the carboxylate linker, and the crystal structures are unsurprisingly very similar (Figure 2 c). The van der Waals interaction with Phe189 is missing, and the 4-oxo group no longer interacts with the W1 structured water or Lys220. Compared with **23**, compound **25** has one extra methylene group in the side chain linker, and the additional flexibility of the propio-

nate group results in two conformations for this moiety in the two active sites of the crystallographic dimer (Figure 2 d). The two conformations appear to be the result of alternate but equally accessible salt bridge interactions with Arg254 and Lys220. Note that each conformation does not affect interactions within the pterin pocket, but does slightly impact the position of the pterin-like scaffold (Figure 2 d).

Compound **17** is identical to **1** save for an extra methylene group in the side chain. The complex structures are nearly identical

except that the carboxylate group more intimately engages the anion pocket and Arg254 (Figure 2 e). Likewise, compound **24** is identical to **19** apart from the additional methylene group, and the structures are again very similar apart from the improved binding within the anion pocket (Figure 2 f). This effect of adding the extra methylene group was anticipated in the design of these compounds.^[21] Note that in both complexes, although the carboxylate moiety interacts more favorably with the anion pocket, alternate hydrogen bonds to Ser218 and Lys220 are lost.

Discussion

Compound **1** was identified as a rather potent inhibitor of DHPS some 30 years ago in a study by researchers at Burroughs Wellcome that was designed to generate pterin-like antibacterial agents as alternatives to the *p*ABA-like sulfa drugs.^[19–21] Although the study generated impressive SAR information, it ultimately suffered from a lack of structural data. We addressed this problem a couple years ago and structurally characterized **1** in the pterin binding pocket of DHPS from *B. anthracis*.^[21] The structure suggested a number of ways in which **1** could be further optimized, and we have reported herein the results of this optimization. Specifically, we designed and synthesized a series of 4,5-dioxo-1,4,5,6-tetrahydropyrimido[4,5-c]pyridazines and characterized their DHPS inhibitory properties by using a direct enzyme assay, ITC and SPR measurements, and crystallography.

Table 2. Summary of ITC and SPR binding data for the most potent inhibitors of *Ba*DHPS.

| Compd | Structure | K_D [μM] | $N^{[a]}$ | ITC data | | | k_a [$\text{M}^{-1}\text{s}^{-1}$] | SPR data ^[b] | | |
|-------|-----------|-------------------------|-----------|------------|--------------|------------|--|---------------------------|------------|-------------------------|
| | | | | ΔH | $-T\Delta S$ | ΔG | | k_d [s^{-1}] | K_D [nM] | $K_{D(\text{eq})}$ [nM] |
| 1 | | 0.124 | 0.8 | -9.8 | 0.39 | -9.41 | $2.84(1) \times 10^5$ | $7.95(4) \times 10^{-2}$ | 280(2) | 267(2) |
| 16 | | ND ^[c] | ND | ND | ND | ND | $3.42(3) \times 10^5$ | $6.94(6) \times 10^{-2}$ | 203(2) | 190(2) |
| 19 | | 0.076 | 0.9 | -8.7 | -0.95 | -9.65 | $3.66(2) \times 10^5$ | $4.39(3) \times 10^{-2}$ | 120(1) | 123(1) |
| 23 | | ND | ND | ND | ND | ND | $4.19(3) \times 10^5$ | $4.35(3) \times 10^{-2}$ | 104(1) | 110(1) |
| 24 | | 0.51 | 0.8 | -7.5 | -1.1 | -8.6 | $6.43(2) \times 10^5$ | $3.39(1) \times 10^{-1}$ | 528(3) | 535(2) |
| 25 | | 0.273 | 0.7 | -10.4 | 1.46 | -8.94 | $4.42(6) \times 10^5$ | $3.14(1) \times 10^{-1}$ | 710(10) | 713(6) |

[a] Stoichiometry of interaction, experimental error: ± 0.01 . [b] Values in parentheses represent the standard error of last reported decimal place. [c] ND: not determined.

Two apparently non-ideal features of **1** were systematically analyzed: the length and branched nature of the carboxylate side chain at the 6-position of the two-ring scaffold, and the presence or absence of the methyl group at the N8 position. In the crystal structure of the complex with compound **1**, the carboxylate group does not optimally fit into the anion pocket, and the N8-methyl group prevents a hydrogen bonding interaction with Asp101. In addition, the methyl group on the carboxylate side chain of **1** was considered favorable due to a van der Waals interaction with the conserved Phe189 that creates part of the pterin binding pocket. Based on our initial SAR analysis,^[21] we would have expected that **24** would display the highest potency, but this is not the case. Although the crystal structure fully supports our prediction, the assay and the physical measurements consistently rank **24** below **1** in potency. Although this is a disappointing and unexpected result, a deeper analysis of the data does reveal possible explanations that will prove invaluable as we move forward with our goal of developing a new DHPS-based lead compound.

Considering only derivatives with one methylene group in the carboxylate side chain, our SAR predictions are fully supported by the data. Thus, removing the N8-methyl group in going from **1** to **19** and from **16** to **23** results in a better inhibitor by all three metrics. Likewise, removing the side chain

methyl group in going from **1** to **16** and **19** to **23** generates less potency. Consistent with these data, compound **16**, which contains the N8 methyl and lacks the side chain methyl group is the least potent inhibitor of the quartet. Inconsistencies appear if the carboxylate side chain is extended by one methylene group. Although the crystal structures clearly show that the extension allows more optimal docking within the anion pocket, this is not reflected by the potency values. Thus, in the pairings **1/17**, **16/18**, **19/24**, and **23/25**, the additional methylene group consistently decreases potency. In the context of the longer side chain, the beneficial effects of the branching methyl group are equivocal; in the **24/25** pairing, SPR suggests tighter binding, whereas ITC and the enzyme assay suggest lower potency. However, it should be noted that the methyl group introduces chirality into the side chain, and measurements with these molecules involve both enantiomers, whereas the crystal structures confirm that only one enantiomer (*R*) binds. Thus, the potency of the chiral compounds is likely to be higher than is apparent from the measurements. Another factor to consider in the loss of the methyl group from the extended side chain is the increased flexibility and the greater entropic penalty associated with its binding and consequent effects on structured water molecules near the site. Figure 2d shows that **25** can indeed adopt two side chain conformations,

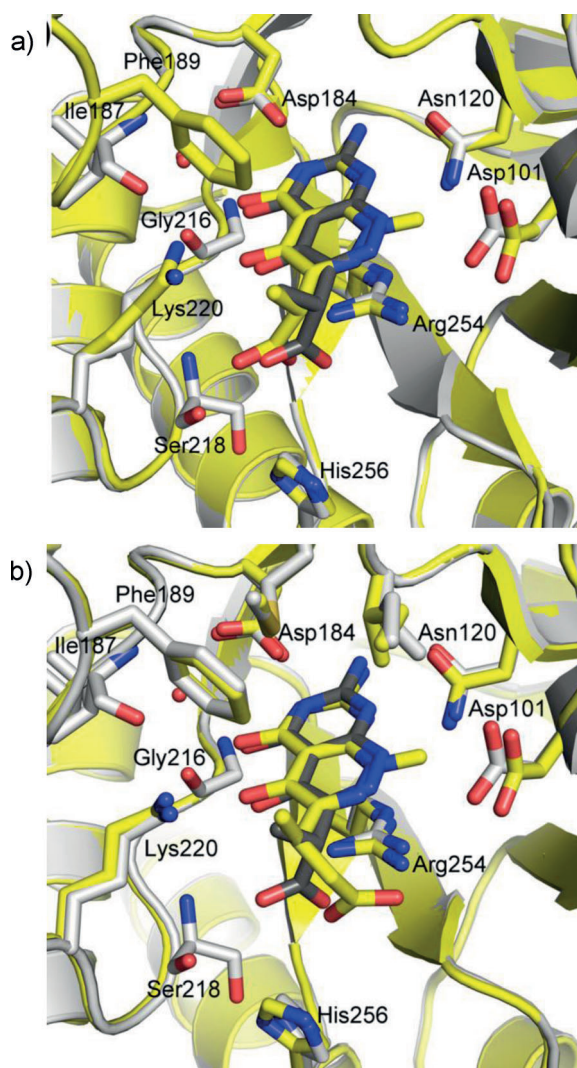


Figure 3. Superimposed crystal structures of *BaDHPS* bound to compounds a) **1** (yellow) and **19** (grey); b) **17** (yellow) and **19** (grey).

and the ITC data reveal that the binding of this compound is associated with the highest entropic penalty.

Notably, the side chain and the terminal carboxylate are clearly beneficial, as evident in comparing **16** with **5** and **25** with **22**. During the course of our studies, we also analyzed compound **21**, which is the ester analogue of compound **24**. The crystal structure of the **21** complex (see Supporting Information figure S4) shows that the ester prevents interaction with Arg254 in the anion pocket, and this is reflected by a significant decrease in inhibitory potency (**21**, IC_{50} : 376 μ M).

The crystal structures reveal that removal of the N8-methyl group does allow the interaction with Asp101 as predicted, but the now smaller pyridazine scaffold moves to optimize this interaction. The precise positioning of the pyridazine scaffold and its interactions within the pterin pocket also appear to be modulated by the presence or absence of the side chain methyl group and the manner in which the terminal carboxylate engages the anion pocket. Although the moderate resolution of our complex structures (2.2–2.5 Å) precludes a detailed

analysis, this movement and the subtle changes in the hydrogen bonding patterns are clearly apparent. These small changes are likely to have significant effects on binding affinity. The described molecules are essentially two linked fragments or pharmacophores that engage adjacent pterin and pyrophosphate binding pockets in DHPS, and the difficulty in connecting these units and capturing the maximum affinity gain is well documented because of subtle but important steric and conformational problems.^[25]

Conclusions

Results from this study suggest that the demethylated pyridazine core is an optimized pterin mimic DHPS inhibitor, but the carboxylate side chain remains an area for further optimization to generate higher-affinity inhibitors. Our recent structural studies have shown that correct occupancy of the pyrophosphate pocket is required for stabilization of the outer loop structure of DHPS,^[16] and hence further efforts are currently underway to generate inhibitors that more fully contact this area.

Experimental Section

Chemistry

Starting materials were purchased from commercial sources except dimethyl 3-methyl-2-oxopentanedioate and were used without further purification. Dimethyl 3-methyl-2-oxopentanedioate was synthesized as previously reported.^[26] The reactions were monitored by thin-layer chromatography (TLC) on pre-coated Merck 60 F₂₅₄ silica gel plates and visualized by UV detection. The purity of final compounds was determined by UPLC/UV/ELSD/MS (see Supporting Information for UPLC/UV/ELSD/MS method). The average UV and ELSD purity is > 95% for all final compounds.^[27] Melting points were obtained on a Thomas Scientific Uni-Melt capillary melting point apparatus (Swedesboro, NJ, USA) and are uncorrected. All ¹H NMR spectra were recorded on a Bruker Ultrashield 400 Plus instrument. Chemical shift values (δ) are expressed in ppm relative to tetramethylsilane as internal standard; s=singlet, d=doublet, t=triplet, q=quartet, m=multiplet, br=broad signal. Coupling constants (*J*) are reported in hertz (Hz).

6-(1-Methylhydrazinyl)pyrimidine-2,4-diamine (3): A stirred mixture of 4-chloro-2,6-diaminopyrimidine (0.694 g, 4.8 mmol) and CH₃NHNH₂ (0.553 g, 12 mmol) in CH₃OH (30 mL) was heated at reflux under N₂ for 18 h. After cooling overnight, the white solid was collected by filtration and dried to give **3** as a white solid (0.198 g, 27%); mp: 215–217 °C; ¹H NMR (400 MHz, [D₆]DMSO): δ =3.06 (s, 3H), 4.33 (brs, 2H), 5.37 (brs, 2H), 5.41 (s, 1H), 5.58 ppm (brs, 2H).

Methyl 5,7-diamino-1-methyl-4-oxo-1,4-dihydropyrimido[4,5-c]-pyridazine-3-carboxylate (4): A mixture of **3** (0.1 g, 0.649 mmol) and diethyl 2-oxomalonate (0.148 mL, 0.908 mmol) in anhydrous CH₃OH (10 mL) was heated at reflux for 72 h under N₂. The solid was filtered out from the hot reaction mixture and washed by filtration to give **4** as a pale-green solid (0.072 g, 44%); mp: ~274 °C (dec.); ¹H NMR (400 MHz, [D₆]DMSO): δ =3.78 (s, 3H), 3.81 (s, 3H), 7.12 (brd, 2H), 7.98 (brs, 1H), 8.82 ppm (brs, 1H).

7-Amino-1-methyl-4,5-dioxo-1,4,5,6-tetrahydropyrimido[4,5-c]pyridazine-3-carboxylic acid (5): A mixture of methyl **4** (0.25 g, 0.999 mmol) and 4 N NaOH (12.5 mL) was stirred at reflux overnight. The white solid was filtered out and then dissolved in hot H₂O. The resulted solution was acidified with dilute HCl to pH 5–6, and the precipitate was collected by filtration and dried to give **5** as a white solid (0.112 g, 47%); mp: >300 °C; ¹H NMR (400 MHz, [D₆]DMSO): δ = 3.89 (s, 3H), 7.22 (brs, 1H), 8.37 ppm (brs, 1H); HRMS *m/z* [M+H]⁺ calcd for C₈H₈N₅O₄: 238.0576, found: 238.0553.

2-Amino-6-(1-methylhydrazinyl)pyrimidin-4(3H)-one (7): A stirred mixture of 2-amino-6-chloropyrimidin-4(3H)-one (1.75 g, 12 mmol) and CH₃NHNH₂ (2.76 g, 60 mmol) in H₂O (90 mL) was heated at reflux for 3 h, and the resulting solution was allowed to stand at room temperature for 5 h before being cooled at 4 °C overnight. The precipitate was collected by filtration and dried under vacuum at 50 °C to give **7** as an off-white solid (1.37 g, 74%); mp: ~275 °C (dec.); ¹H NMR (400 MHz, [D₆]DMSO): δ = 3.11 (s, 3H), 4.45 (brs, 2H), 4.99 (s, 1H), 6.17 (brs, 2H), 9.84 ppm (brs, 1H).

2-Amino-6-(1-benzylhydrazinyl)pyrimidin-4(3H)-one (8): A stirred mixture of 2-amino-6-chloropyrimidin-4(3H)-one (0.4 g, 2.75 mmol) and BnNHNH₂·2HCl (1.072 g, 5.50 mmol) along with Et₃N (2.857 mL, 20.61 mmol) in H₂O (15 mL) was heated at reflux overnight. The reaction mixture was cooled to room temperature, and the solid was filtered out and dried over P₂O₅ to give **8** as an off-white solid (220 mg, 35%); mp: ~280 °C (dec.); ¹H NMR (400 MHz, [D₆]DMSO): δ = 4.36 (brs, 2H), 4.86 (s, 2H), 5.05 (s, 1H), 6.22 (brs, 2H), 7.19–7.33 (m, 5H), 9.79 ppm (brs, 1H).

General method for the synthesis of 9–15: A mixture of **7** (or **8**) and the appropriate keto ester in solvent (distilled H₂O, expect **9** and **12**, which were obtained from anhydrous CH₃OH) was heated at reflux for 1.5–24 h. The resulting precipitate was collected by filtration from the hot mixture, washed with reaction solvent, and dried under vacuum over P₂O₅ to give target compounds **9–11** (or **12–15**).

Ethyl 2-(7-amino-1-methyl-4,5-dioxo-1,4,5,6-tetrahydropyrimido[4,5-c]pyridazin-3-yl)acetate (9): Compound **9** was obtained from **7** (0.50 g, 3.22 mmol) and diethyl 2-oxosuccinate (1.03 g, 0.904 mL, 5.48 mmol) by following the general method described above after 3 h as a white solid (0.355 g, 39%); mp: >300 °C; ¹H NMR (400 MHz, [D₆]DMSO): δ = 1.18 (t, *J* = 7.2 Hz, 3H), 3.47 (s, 2H), 3.73 (s, 3H), 4.06 (q, *J* = 7.2 Hz, 2H), 10.89 ppm (brs, 1H).

Methyl 3-(7-amino-1-methyl-4,5-dioxo-1,4,5,6-tetrahydropyrimido[4,5-c]pyridazin-3-yl)butanoate (10): Compound **10** was obtained from **7** (0.08 g, 0.43 mol) and dimethyl 3-methyl-2-oxopentanedioate (0.07 g, 0.43 mmol) by following the general method described above after 3 h as a light-pink solid (0.03 g, 27%); mp: >300 °C; ¹H NMR (400 MHz, [D₆]DMSO): δ = 1.09 (d, *J* = 6.9 Hz, 3H), 2.44 (dd, *J* = 15.9, 7.3 Hz, 1H), 2.70 (dd, *J* = 15.9, 7.5 Hz, 1H), 3.48–3.55 (m, 1H), 3.56 (s, 3H), 3.69 (s, 3H), 10.80 ppm (s, 1H).

Methyl 3-(7-amino-1-methyl-4,5-dioxo-1,4,5,6-tetrahydropyrimido[4,5-c]pyridazin-3-yl)propanoate (11): Compound **11** was obtained from **7** (0.8 g, 5.16 mmol) and dimethyl 2-oxoglutarate (0.896 mL, 6.19 mmol) by following the general method described above after 1.5 h as a yellow solid (0.71 g, 49%); mp: >300 °C; ¹H NMR (400 MHz, [D₆]DMSO): δ = 2.59 (t, *J* = 7.6 Hz, 2H), 2.57 (t, *J* = 7.6 Hz, 2H), 3.59 (s, 3H), 3.69 (s, 3H), 10.81 ppm (brs, 1H).

Ethyl 2-(7-amino-1-benzyl-4,5-dioxo-1,4,5,6-tetrahydropyrimido[4,5-c]pyridazin-3-yl)acetate (12): Compound **12** was obtained from **8** (0.3 g, 1.297 mmol) and diethyl 2-oxosuccinate (0.642 mL, 3.89 mmol) by following the general method described above after

two days as a light-pink solid (0.189 g, 41%); mp: >300 °C; ¹H NMR (400 MHz, [D₆]DMSO): δ = 1.15 (t, *J* = 7.2 Hz, 3H), 3.49 (s, 2H), 4.04 (q, *J* = 7.2 Hz, 2H), 5.39 (s, 2H), 7.26–7.35 (m, 5H), 10.94 ppm (brs, 1H).

Ethyl 2-(7-amino-1-benzyl-4,5-dioxo-1,4,5,6-tetrahydropyrimido[4,5-c]pyridazin-3-yl)propanoate (13): Compound **13** was obtained from **8** (0.150 g, 0.649 mmol) and diethyl 2-methyl-3-oxosuccinate (0.240 mL, 1.297 mmol) by following the general method described above after 3 h as an off-white solid (0.185 g, 77%); mp: >300 °C; ¹H NMR (400 MHz, [D₆]DMSO): δ = 1.09 (t, *J* = 7.2 Hz, 3H), 1.28 (d, *J* = 7.2 Hz, 3H), 3.85 (t, *J* = 7.2 Hz, 2H), 3.97–4.03 (m, 2H), 5.38 (q, *J* = 14.8 Hz, 2H), 7.26–7.36 (m, 5H), 10.92 ppm (brs, 1H).

Methyl 3-(7-amino-1-benzyl-4,5-dioxo-1,4,5,6-tetrahydropyrimido[4,5-c]pyridazin-3-yl)butanoate (14): Compound **14** was obtained from **8** (0.29 g, 1.26 mol) and dimethyl 3-methyl-2-oxopentanedioate (0.26 g, 1.38 mmol) by following the general method described above after 3 h as a white solid (0.18 g, 39%); mp: >300 °C; ¹H NMR (400 MHz, [D₆]DMSO): δ = 1.08 (d, *J* = 6.9 Hz, 3H), 2.34 (dd, *J* = 16.1, 7.0 Hz, 1H), 2.42–2.48 (m, 1H), 2.69 (m, 1H), 3.45 (s, 3H), 5.16–5.50 (m, 2H), 7.19–7.42 (m, 5H), 10.84 (s, 1H), 12.02 ppm (s, 1H).

Methyl 3-(7-amino-1-benzyl-4,5-dioxo-1,4,5,6-tetrahydropyrimido[4,5-c]pyridazin-3-yl)propanoate (15): Compound **15** was obtained from **8** (0.3 g, 1.297 mmol) and dimethyl 2-oxopentanedioate (0.469 mL, 3.24 mmol) by following the general method described above after 3 h as an off-white solid (0.394 g, 85%); mp: >300 °C; ¹H NMR (400 MHz, [D₆]DMSO): δ = 2.60 (t, *J* = 7.2 Hz, 2H), 2.78 (t, *J* = 7.2 Hz, 2H), 3.49 (s, 3H), 5.32 (s, 2H), 7.26–7.35 (m, 5H), 10.87 ppm (brs, 1H).

General method for the synthesis of 16–18: A suspension of compounds **9–11** in THF (10 mL) and 1 N NaOH (6 mL) was stirred at room temperature overnight. The solvent was removed by evaporation under vacuum to a small volume. The solution was neutralized with dilute HCl to pH 5–6. The fluffy solid was filtered out and dried over P₂O₅ to give target compounds **16–18**.

2-(7-Amino-1-methyl-4,5-dioxo-1,4,5,6-tetrahydropyrimido[4,5-c]pyridazin-3-yl)acetic acid (16): Compound **16** was obtained from **9** (0.1 g, 0.358 mmol) by following the general method described above as an off-white solid (0.065 g, 72%); mp: >300 °C; ¹H NMR (400 MHz, [D₆]DMSO): δ = 3.41 (s, 2H), 3.73 (s, 3H), 10.89 (s, 1H), 12.36 ppm (s, 1H); HRMS *m/z* [M+H]⁺ calcd for C₉H₁₀N₅O₄: 252.0733, found: 252.0701.

3-(7-Amino-1-methyl-4,5-dioxo-1,4,5,6-tetrahydropyrimido[4,5-c]pyridazin-3-yl)butanoic acid (17): Compound **17** was obtained from **11** (0.035 g, 0.12 mmol) by following the general method described above as a off-white solid (0.021 g, 63%); mp: ~295 °C (dec.); ¹H NMR (400 MHz, [D₆]DMSO): δ = 1.08 (d, *J* = 6.9 Hz, 3H), 2.33 (dd, *J* = 16.0, 7.4 Hz, 1H), 2.64 (dd, *J* = 16.1, 7.4 Hz, 1H), 3.50 (h, *J* = 7.1 Hz, 1H), 3.70 (s, 3H), 10.79 (s, 1H), 12.01 ppm (s, 1H); HRMS *m/z* [M+H]⁺ calcd for C₁₁H₁₄N₅O₄: 280.1046, found: 280.1041.

3-(7-Amino-1-methyl-4,5-dioxo-1,4,5,6-tetrahydropyrimido[4,5-c]pyridazin-3-yl)propanoic acid (18): Compound **18** was obtained from **10** (0.3 g, 1.02 mmol) by following the general method described above as a yellow solid (0.258 g, 95%); mp: >300 °C; ¹H NMR (400 MHz, [D₆]DMSO): δ = 2.52 (t, *J* = 7.6 Hz, 2H), 2.78 (t, *J* = 7.6 Hz, 2H), 3.49 (s, 3H), 7.30 (brs, 2H), 10.99 (brs, 1H), 12.10 ppm (brs, 1H); HRMS *m/z* [M+H]⁺ calcd for C₁₀H₁₂N₅O₄: 266.0889, found: 266.0877.

2-(7-Amino-4,5-dioxo-1,4,5,6-tetrahydropyrimido[4,5-c]pyridazin-3-yl)propanoic acid (19): A mixture of **13** (0.2 g, 0.541 mmol) and AlCl_3 (0.289 g, 2.17 mmol) in PhCH_3 (anhyd, 30 mL) was heated at reflux for 3 h. The solvent was decanted, and the residue was dissolved in DMSO and purified by LC (Waters Prep LC System) with H_2O (0.1% HCOOH) and CH_3OH (0.1% HCOOH) as eluent to give **19** as a light-yellow solid (0.035 g, 27%); mp: $>300^\circ\text{C}$; $^1\text{H NMR}$ (400 MHz, $[\text{D}_6]\text{DMSO}$): $\delta = 1.28$ (d, $J = 7.2$ Hz, 3H), 3.80 (q, $J = 7.2$ Hz, 1H), 7.08 (brs, 2H), 10.76 (brs, 1H), 12.22 (brs, 1H), 12.62 ppm (brs, 1H); HRMS m/z $[\text{M}-\text{H}]^-$ calcd for $\text{C}_9\text{H}_8\text{N}_5\text{O}_4$: 250.0576, found: 250.0595.

General method for the synthesis of 20–22: A solution of **12** (or **14–15**) and 10% Pd/C (1:1 w/w) in HCOOH (10 mL) was stirred at room temperature under N_2 for 24 h. The reaction solution was filtered through a Celite pad, and the filter cake was washed with warm HCOOH (10 mL). The solvent was removed under reduced pressure to the minimum volume, and the residue was purified by LC (Waters Prep LC System) with H_2O (0.1% HCOOH) and CH_3OH (0.1% HCOOH) as eluent to give compound **20** (or **21–22**).

Ethyl 2-(7-amino-4,5-dioxo-1,4,5,6-tetrahydropyrimido[4,5-c]pyridazin-3-yl)acetate (20): Compound **20** was obtained from **12** (0.587 g, 1.652 mmol) by following the general method described above as a white solid (0.07 g, 16%); mp: $>300^\circ\text{C}$; $^1\text{H NMR}$ (400 MHz, $[\text{D}_6]\text{DMSO}$): $\delta = 1.17$ (t, $J = 7.2$ Hz, 3H), 3.47 (s, 2H), 4.06 (q, $J = 7.2$ Hz, 2H), 7.15 (brs, 2H), 10.89 (brs, 1H), 12.70 ppm (brs, 1H).

Methyl 3-(7-amino-4,5-dioxo-1,4,5,6-tetrahydropyrimido[4,5-c]pyridazin-3-yl)butanoate (21): Compound **21** was obtained from **14** (0.11 g, 0.30 mmol) by following the general method described above as a white solid (0.04 g, 48%); mp: $>300^\circ\text{C}$; $^1\text{H NMR}$ (400 MHz, $[\text{D}_6]\text{DMSO}$): $\delta = 1.08$ (d, $J = 6.9$ Hz, 3H), 2.44 (dd, $J = 15.9$, 7.1 Hz, 1H), 2.71 (dd, $J = 15.9$, 7.7 Hz, 1H), 3.54 (m, 1H), 3.55 (s, 3H), 7.02 (brs, 2H), 10.70 (s, 1H), 12.51 ppm (s, 1H).

Methyl 3-(7-amino-4,5-dioxo-1,4,5,6-tetrahydropyrimido[4,5-c]pyridazin-3-yl)propanoate (22): Compound **22** was obtained from **15** (0.3 g, 0.84 mmol) by following the general method described above as a white solid (0.025 g, 11%); mp: $>300^\circ\text{C}$; $^1\text{H NMR}$ (400 MHz, $[\text{D}_6]\text{DMSO}$): $\delta = 2.61$ (t, $J = 6.8$ Hz, 2H), 2.76 (t, $J = 6.8$ Hz, 2H), 3.58 (s, 3H), 7.11 (brs, 2H), 10.92 (brs, 1H), 12.52 ppm (brs, 1H).

2-(7-Amino-4,5-dioxo-1,4,5,6-tetrahydropyrimido[4,5-c]pyridazin-3-yl)acetic acid (23): Compound **23** was obtained from **20** (0.025 g, 0.094 mmol) by following the general method described for the synthesis of **16–18** as a white solid (0.02 g, 89%); mp: $>300^\circ\text{C}$; $^1\text{H NMR}$ (400 MHz, $[\text{D}_6]\text{DMSO}$): $\delta = 3.40$ (s, 2H), 7.15 (brs, 2H), 10.74 (s, 1H), 12.31 (brs, 1H), 12.62 ppm (s, 1H); HRMS m/z $[\text{M}+\text{H}]^+$ calcd for $\text{C}_8\text{H}_8\text{N}_5\text{O}_4$: 238.0576, found: 238.0553.

3-(7-Amino-4,5-dioxo-1,4,5,6-tetrahydropyrimido[4,5-c]pyridazin-3-yl)butanoic acid (24): Compound **24** was obtained from **21** (0.013 mg, 0.05 mmol) by following the general method described for the synthesis of **16–18** as a white solid (0.005 mg, 41%); mp: $>300^\circ\text{C}$; $^1\text{H NMR}$ (400 MHz, $[\text{D}_6]\text{DMSO}$): $\delta = 1.07$ (d, $J = 6.9$ Hz, 3H), 2.33 (dd, $J = 15.6$, 7.1 Hz, 1H), 2.63 (dd, $J = 16.7$, 7.7 Hz, 1H), 3.50 (q, $J = 7.0$ Hz, 1H), 10.65 (s, 1H), 11.97 (s, 1H), 12.49 ppm (s, 1H); HRMS m/z $[\text{M}+\text{H}]^+$ calcd for $\text{C}_{10}\text{H}_{12}\text{N}_5\text{O}_4$: 266.0889, found: 266.0877.

3-(7-Amino-4,5-dioxo-1,4,5,6-tetrahydropyrimido[4,5-c]pyridazin-3-yl)propanoic acid (25): Compound **25** was obtained from **23** (0.02 g, 0.075 mmol) by following the general method described for the synthesis of **16–18** as a white solid (0.012 g, 61%); mp:

$>300^\circ\text{C}$; $^1\text{H NMR}$ (400 MHz, $[\text{D}_6]\text{DMSO}$): $\delta = 2.52$ (t, $J = 7.2$ Hz, 2H), 2.72 (t, $J = 7.2$ Hz, 2H), 6.99 (brs, 2H), 10.69 (s, 1H), 12.06 (s, 1H), 12.53 ppm (s, 1H); HRMS m/z $[\text{M}+\text{H}]^+$ calcd for $\text{C}_9\text{H}_{11}\text{N}_5\text{O}_4$: 252.0733, found: 252.0701.

Enzyme assays

DHPS activity was measured in a 30 μL reaction containing 5 μM $[\text{C}^{14}]\text{pABA}$, 10 μM 6-hydroxymethyl-7,8-dihydropterin diphosphate, 10 mM MgCl_2 , 2% DMSO, 50 mM HEPES pH 7.6, and 10 ng DHPS.^[28,29] After 30 min incubation at 37°C , the reactions were stopped by the addition of 1 μL 50% acetic acid in an ice bath. The labeled product of the reaction, $[\text{C}^{14}]\text{dihydropteroate}$, was separated from $[\text{C}^{14}]\text{pABA}$ by TLC. Aliquots (15 μL) of the reaction mixture were spotted onto Polygram TLC plates (CEL 300 PEI) purchased from Macherey–Nagel and developed with ascending chromatography in 100 mM phosphate buffer, pH 7.0. The plates were scanned using a Typhoon (GE Healthcare) and analyzed with ImageQuant TL. Inhibitor compounds were dissolved in DMSO, and inhibition was tested at 500 or 250 μM , depending on solubility. The final concentration of DMSO in the reaction mixture was 2%. To determine the 50% inhibitory concentration (IC_{50}) values, DHPS activities were measured in the presence of various concentrations of the compounds using the conditions described above, but with 5 ng DHPS.

Crystallography

Compounds were dissolved in the crystallization mother liquor (1.45 M Li_2SO_4 , 0.1 M Bis-Tris propane pH 9.0) until saturated. Co-crystal structures of *B. anthracis* DHPS with compounds **17**, **19**, **21**, **23**, **24**, and **25** were obtained by soaking the small molecules into pre-grown crystals, which were obtained as previously described.^[9] After a soaking period of 12 h, the crystals were cryoprotected by a brief immersion in a mixture of 50% paratone-N/50% mineral oil and flash-frozen in liquid nitrogen. Diffraction data were collected at the SER-CAT 22-ID and 22-BM beamlines of the Advanced Photon Source and processed using HKL2000.^[30] Structures were refined using re mac5,^[31] CNS,^[32] and Phenix,^[33] and model building was performed using the programs Coot^[34] and O.^[35] Figures 2 and 3 (as well as figures S4 and S5 in the Supporting Information) were rendered with PyMOL.^[36] The atomic coordinates for the DHPS inhibitor-bound structures have been deposited into the RCSB Protein Data Bank with the following PDB IDs: **23**, 4DAI; **19**, 4DAF; **17**, 4D9P; **24**, 4D8Z; **21**, 4D8A; **25**, 4DB7. Table 3 lists crystallographic refinement statistics for these.

Isothermal titration calorimetry

The purified *B. anthracis* DHPS protein was dialyzed against 50 mM HEPES pH 7.6, 5 mM MgCl_2 . ITC titrations were performed in 5% DMSO, 40 mM HEPES pH 7.6, 4 mM MgCl_2 at 25°C . Nineteen injections (2 μL) of each ligand (200 μM solution) were added to 203 μL protein solution (20 μM). ITC titrations were performed on an Auto-iTC200 isothermal titration calorimeter (MicroCal), and data were analyzed with MicroCal Origin 7.0 software using a one-site binding model.

SPR methods

Binding studies were performed at 25°C using a BIACORE T100 (GE Healthcare) surface plasmon resonance (SPR) instrument; $10\times$

Table 3. Crystallographic statistics of refinement.^[a]

| Parameter | 17 | 19 | 21 | 23 | 24 | 25 |
|----------------------|----------|----------|----------|----------|----------|----------|
| Resolution range [Å] | 87.0–2.2 | 30.0–2.5 | 35.6–2.2 | 30.0–2.5 | 29.0–2.2 | 30.0–2.4 |
| R_{work} | 0.233 | 0.257 | 0.219 | 0.253 | 0.216 | 0.257 |
| R_{free} | 0.270 | 0.286 | 0.259 | 0.282 | 0.259 | 0.283 |

[a] See Supporting Information tables S2 and S3 for further crystallographic statistics of data collection and refinement.

His-BaDHPS was immobilized on a nitrilotriacetic acid-derivatized carboxymethyl-dextran-coated gold surface (NTA Chip, GE Healthcare) at a level of ~5360 RU using the manufacturer's protocol. The kinetics of association and dissociation were monitored at a flow rate of 100 $\mu\text{L min}^{-1}$. Compounds were prepared in 20 mM Tris pH 7.7, 150 mM NaCl, 5 mM MgCl₂, 1 mM TCEP, 0.005% Tween 20, and 5% DMSO as threefold serial dilutions decreasing from 3 μM to 37 nM for **1**, 9 μM to 111 nM for **19**, and 1 μM to 12.3 nM for **22**. Each compound was injected in triplicate at each concentration. The data were processed, double-referenced, solvent corrected, and analyzed by kinetic and equilibrium affinity methods using the software package Scrubber2 (version 2.0b, BioLogig Software).

Acknowledgements

Funding for this research was provided by National Institutes of Health grant A1070721, Cancer Center core grant CA21765, and the American Lebanese Syrian Associated Charities (ALSAC). We thank Matthew Frank from the Department of Infectious Diseases at St. Jude Children's Research Hospital for help with the radiometric enzyme inhibition assay. We also thank Jerrod Scarborough, Drs. Lei Yang, and Bing Yan from the Department of Chemical Biology and Therapeutics at St. Jude Children's Research Hospital for their help in the analysis and purification of final compounds, and Brett Waddell for assistance with the SPR experiments. Crystallography data were collected at Southeast Regional Collaborative Access Team (SER-CAT) 22-ID and 22-BM beamlines at the Advanced Photon Source, Argonne National Laboratory. Supporting institutions may be found at <http://www.ser-cat.org/members.html>. Use of the Advanced Photon Source was supported by the US Department of Energy, Office of Science, Office of Basic Energy Sciences, under Contract No. W-31-109-Eng-38.

Keywords: antimicrobial agents · dihydropteroate synthase · heterocycles · structure-based drug design

- [1] A. K. Miller, *Proc. Natl. Acad. Sci. USA* **1944**, *57*, 151–153.
 [2] D. D. Woods, *Br. J. Exp. Pathol.* **1940**, *21*, 74–90.
 [3] O. Skold, *Drug Resist. Updates* **2000**, *3*, 155–160.
 [4] B.-E. Wiholm, S. Emanuelsson, *Eur. J. Haematol.* **1996**, *57*, 42–46.
 [5] A. Bermingham, J. P. Derrick, *BioEssays* **2002**, *24*, 637–648.
 [6] H. W. Boucher, G. H. Talbot, J. S. Bradley, J. E. Edwards, D. Gilbert, L. B. Rice, M. Scheld, B. Spellberg, J. Bartlett, *Clin. Infect. Dis.* **2009**, *48*, 1–12.

- [7] D. A. Dibbern, Jr., A. Montanaro, *Ann. Allergy Asthma Immunol.* **2008**, *100*, 91–101.
 [8] A. Achari, D. Somers, J. N. Champness, P. K. Bryant, J. Rosemond, D. K. Stammers, *Nat. Struct. Mol. Biol.* **1997**, *4*, 490–497.
 [9] K. Babaoglu, J. Qi, R. E. Lee, S. W. White, *Structure* **2004**, *12*, 1705–1717.
 [10] A. M. Baca, R. Sirawaraporn, S. Turley, W. Sirawaraporn, W. G. J. Hol, *J. Mol. Biol.* **2000**, *302*, 1193–1212.
 [11] Y. Haasum, K. Strom, R. Wehelie, V. Luna, M. C. Roberts, J. P. Maskell, L. M. C. Hall, G. Swedberg, *Antimicrob. Agents Chemother.* **2001**, *45*, 805–809.
 [12] I. C. Hampele, A. D'Arcy, G. E. Dale, D. Kostrewa, J. Nielsen, C. Oefner, M. G. P. Page, H.-J. Schonfeld, D. Stuber, R. L. Then, *J. Mol. Biol.* **1997**, *268*, 21–30.
 [13] K. E. Hevener, W. Zhao, D. M. Ball, K. Babaoglu, J. Qi, S. W. White, R. E. Lee, *J. Chem. Inf. Model.* **2009**, *49*, 444–460.
 [14] M. C. Lawrence, P. Iliades, R. T. Fernley, J. Berglez, P. A. Pilling, I. G. Maccreadie, *J. Mol. Biol.* **2005**, *348*, 655–670.
 [15] C. Levy, D. Minnis, J. P. Derrick, *Biochem. J.* **2008**, *412*, 379–388.
 [16] M.-K. Yun, Y. Wu, Z. Li, Y. Zhao, M. B. Waddell, A. M. Ferreira, R. E. Lee, D. Bashford, S. W. White, *Science* **2012**, *335*, 1110–1114.
 [17] Y. Zhao, D. Hammoudeh, W. Lin, S. Das, M.-K. Yun, Z. Li, E. Griffith, T. Chen, S. W. White, R. E. Lee, *Bioconjugate Chem.* **2011**, *22*, 2110–2117.
 [18] J. Qi, K. G. Virga, S. Das, Y. Zhao, M.-K. Yun, S. W. White, R. E. Lee, *Bioorg. Med. Chem.* **2011**, *19*, 1298–1305.
 [19] R. W. Morrison, Jr., W. R. Mallory, V. L. Styles, "Pyrimido[4,5-c]pyridazines, Their Use in Pharmaceutical Compositions, Process and Intermediates for Their Preparation", EP 0000383 (A1), **1979**.
 [20] R. W. Morrison, W. R. Mallory, V. L. Styles, *J. Org. Chem.* **1978**, *43*, 4844–4849.
 [21] K. E. Hevener, M. K. Yun, J. J. Qi, I. D. Kerr, K. Babaoglu, J. G. Hurdle, K. Balakrishna, S. W. White, R. E. Lee, *J. Med. Chem.* **2010**, *53*, 166–177.
 [22] A. L. Campbell, D. R. Pilipauskas, I. K. Khanna, R. A. Rhodes, *Tetrahedron Lett.* **1987**, *28*, 2331–2334.
 [23] B. ElAmin, G. M. Anantharamaiah, G. P. Royer, G. E. Means, *J. Org. Chem.* **1979**, *44*, 3442–3444.
 [24] J. E. Ladbury, G. Klebe, E. Freire, *Nat. Rev. Drug Discovery* **2010**, *9*, 23–27.
 [25] P. J. Hajduk, J. Greer, *Nat. Rev. Drug Discovery* **2007**, *6*, 211–219.
 [26] C. Milne, A. Powell, J. Jim, M. Al Nakeeb, C. P. Smith, J. Micklefield, *J. Am. Chem. Soc.* **2006**, *128*, 11250–11259.
 [27] A. Lemoff, B. Yan, *J. Comb. Chem.* **2008**, *10*, 746–751.
 [28] T. V. Aspinall, D. H. M. Joynson, E. Guy, J. E. Hyde, P. F. G. Sims, *J. Infect. Dis.* **2002**, *185*, 1637–1643.
 [29] H. G. Vinnicombe, J. P. Derrick, *Biochem. Biophys. Res. Commun.* **1999**, *258*, 752–757.
 [30] Z. Otwinowski, W. Minor, C. W. Carter, Jr., *Methods Enzymol.* **1997**, *276*, 307–326.
 [31] G. N. Murshudov, A. A. Vagin, E. J. Dodson, *Acta Crystallogr. Sect. D* **1997**, *53*, 240–255.
 [32] A. T. Brünger, P. D. Adams, G. M. Clore, W. L. DeLano, P. Gros, R. W. Grosse-Kunstleve, J. S. Jiang, J. Kuszewski, M. Nilges, N. S. Pannu, *Acta Crystallogr. Sect. D* **1998**, *54*, 905–921.
 [33] P. D. Adams, P. V. Afonine, G. Bunkóczi, V. B. Chen, I. W. Davis, N. Echols, J. J. Headd, L.-W. Hung, G. J. Kapral, R. W. Grosse-Kunstleve, A. J. McCoy, N. W. Moriarty, R. Oeffner, R. J. Read, D. C. Richardson, J. S. Richardson, T. C. Terwilliger, P. H. Zwart, *Acta Crystallogr. Sect. D* **2010**, *66*, 213–221.
 [34] P. Emsley, K. Cowtan, *Acta Crystallogr. Sect. D* **2004**, *60*, 2126–2132.
 [35] G. J. Kleywegt, T. Alwyn Jones, R. M. S. Charles, W. Carter, Jr., *Methods Enzymol.* **1997**, *277*, 208–230.
 [36] W. L. DeLano, *The PyMOL Molecular Graphics System*, 1.3, DeLano Scientific, San Carlos, CA (USA), **2002**.

Received: January 24, 2012

Revised: February 27, 2012

Published online on March 13, 2012